Periodic waves in fiber Bragg gratings

K. W. Chow,[1] Ilya M. Merhasin,[2] Boris A. Malomed,[3] K. Nakkeeran,[4] K. Senthilnathan,[5] and P. K. A. Wai[5]

[1]*Department of Mechanical Engineering, University of Hong Kong, Pokfulam Road, Hong Kong*
[2]*Department of Electrical and Electronics Engineering, The University Center of Judea and Samaria, Ariel, Israel*
[3]*Department of Physical Electronics, School of Electrical Engineering, Faculty of Engineering, Tel Aviv University,*
Tel Aviv 69978, Israel
[4]*School of Engineering, King's College, University of Aberdeen, Aberdeen AB24 3UE, Scotland, United Kingdom*
[5]*Photonics Research Center and Department of Electronic and Information Engineering, The Hong Kong Polytechnic University,*
Hung Hom, Kowloon, Hong Kong

We construct two families of exact periodic solutions to the standard model of fiber Bragg grating (FBG) with Kerr nonlinearity. The solutions are named "sn" and "cn" waves, according to the elliptic functions used in their analytical representation. The sn wave exists only inside the FBG's spectral bandgap, while waves of the cn type may only exist at negative frequencies ($\omega < 0$), both inside and outside the bandgap. In the long-wave limit, the sn and cn families recover, respectively, the ordinary gap solitons, and (unstable) antidark and dark solitons. Stability of the periodic solutions is checked by direct numerical simulations and, in the case of the sn family, also through the calculation of instability growth rates for small perturbations. Although, rigorously speaking, all periodic solutions are unstable, a subfamily of practically stable sn waves, with a sufficiently large spatial period and $\omega > 0$, is identified. However, the sn waves with $\omega < 0$, as well as all cn solutions, are strongly unstable.

I. INTRODUCTION

Periodically structured optical media have been in the focus of research activity for many years, due to their versatile technological applications in the fields of telecommunications and sensor systems [1], and also as a subject of fundamental studies [2]. At the early stage of the work in this area, the pioneering contribution by Winful, Marburger, and Garmire [3] laid the groundwork for extensive theoretical activities exploring nonlinear pulse propagation in one-dimensional periodic structures known as fiber Bragg gratings (FBGs). These structures are based on the periodic modulation of the local refractive index in the axial direction. A characteristic feature of FBGs is a stopband, alias photonic bandgap, in their linear-propagation spectrum. The bandgap is induced by the resonant coupling between the forward- and backward-propagating waves due to the Bragg resonance.

The role of the Kerr nonlinearity in the light transmission through FBGs was first considered in Ref. [3], where the optical bistability in nonlinear FBGs was predicted, and analytical expressions were derived for the transmissivity, in terms of elliptic functions. Similar solutions have found other applications to optics, such as the bistability of nonlinear optical waves in cholesteric liquid crystals [4], waves generated by the four-wave mixing [5], and nonlinear states in FBGs produced by the bidirectional illumination [6]. The possibility of the optical-pulse compression and soliton propagation in FBGs with the carrier frequency set outside the photonic bandgap were highlighted too [7]. Then, standing solitary waves, i.e., immobile optical solitons in FBGs, whose carrier frequency lies within the bandgap [hence the name of gap solitons (GSs) is often applied to these localized states], had been predicted in Refs. [8–10]. These works

demonstrated that the local phase in the gap-soliton solutions satisfies the stationary double sine-Gordon equation, which admits well-known kink and antikink solutions. The amplitude of the electromagnetic field in the resulting solution is a localized function, with a more complex structure than the simple hyperbolic secant commonly known in terms of nonlinear-Schrödinger solitons. A general family of analytical soliton solutions of the standard FBG model, including both standing and moving pulses, was reported in Refs. [11] and [12]. In the latter work, the solitons were found using the similarity of the equations to the massive Thirring model, known in field theory. The family of the FBG solitons features two nontrivial parameters, that account for the amplitude (or frequency) and velocity of the solitons (it is interesting to mention that a part of this family, namely, the solitons with an arbitrary velocity and zero intrinsic frequency, were found in an earlier work [8]).

Experimentally, FBG solitons were created in a short piece of a fiber, less than 10 cm long [13]. Originally, the solitons were quite fast, featuring the velocity no smaller than half the speed of light in the fiber. However, using the possibility to slow down the solitons in an apodized FBG (that with the local Bragg reflectivity increasing along the propagation length), much slower solitons (with the velocity equal 1/6 of the light speed, which is not a limit) have been demonstrated recently [14]. Before that, the apodization was used to facilitate coupling of soliton-forming light pulses into the FBG [13].

Unlike the abovementioned integrable Thirring model, the coupled-mode equations (CMEs) which constitute the FBG model, are not integrable; in that sense, the abovementioned solutions are not true solitons, but rather "solitary waves," in terms of the rigorous mathematical classification. In particular, the lack of integrability of the CMEs is manifested by simulations of collisions between moving solitons: the colli-

sions are inelastic, and may lead to fusion of colliding pulses into a single one [15]. Nevertheless, in addition to the two-parameter soliton family, the FBG-CME system may admit other physically relevant exact solutions. The objective of the present work is to report analytical periodic-wave solutions, and, which is crucially important to the physical applications, to examine their stability by means of both the rigorous analysis of linearized equations for small perturbations, and in direct simulations. We find two families of the solutions, one of them similar to but distinct from the original solutions reported in Ref. [3]. Note that the stability of the periodic solutions was not systematically explored before (modulational instability of uniform states was simulated in Ref. [16], and studied in detail in Ref. [17]; instability of periodic solutions in a model with a delayed nonlinear response was demonstrated in Ref. [18]). We conclude that, strictly speaking, all the periodic solutions are unstable, but some of them may feature an extremely weak instability, thus suggesting a possibility to create new virtually stable nonlinear patterns in the experiment.

The paper is organized as follows. In Sec. II, we introduce the standard CME system for the FBG, and give two families of exact periodic solutions expressed in terms of Jacobi's elliptic functions sn and cn. The long-wave limit for these periodic waves is considered too (the sn solutions degenerate into the GS, while the cn waves take the limit form of an antidark or dark soliton) In Sec. III, the stability of the periodic waves is investigated by means of linearized equations for small perturbations, and in direct simulations. The paper is concluded by Sec. IV (where, in particular, we mention applications of the obtained solutions in other areas).

II. PERIODIC SOLUTIONS TO THE COUPLED-MODE EQUATIONS

The standard model of the Kerr-nonlinear optical fiber with the Bragg grating written in its cladding is based on the system of CMEs for amplitudes of counterpropagating waves $U(x,t)$ and $V(x,t)$, which are coupled linearly by the Bragg reflection, and nonlinearly by the cross-phase modulation (XPM), and also take into regard the self-phase modulation (SPM) effect [19]. In the scaled form, the equations are

$$iU_t + iU_x + \left(\frac{1}{2}|U|^2 + |V|^2\right)U + \kappa V = 0,$$

$$iV_t - iV_x + \left(\frac{1}{2}|V|^2 + |U|^2\right)V + \kappa U = 0, \quad (1)$$

where x and t are the coordinate along the fiber and time, and κ the Bragg reflectivity (which may be defined to be positive), while the group velocity of light and the overall Kerr coefficient are scaled to be 1. In fact, one may additionally normalize Eqs. (1) so as to set $\kappa \equiv 1$; nevertheless, we prefer to keep this coefficient in the equations, as the results may then be easily generalized to the case of the abovementioned apodization, by replacing constant κ with a slowly varying function $\kappa(x)$. In the latter case, exact solutions pertaining to $\kappa = $const may be used as a basis for a perturbative treatment

[20]. In physical units, the Bragg-reflection length, which is estimated as $\sim 1/\kappa$ in terms of Eqs. (1), usually takes values $\simeq 1$ mm, and the corresponding scaled time unit $t=1$ corresponds to $\simeq 10$ ps [1].

As said above, a two-parameter family of soliton solutions to Eqs. (1) is available in an exact form [8–12]. The stability of the solitons was first studied by means of the variational approximation [21], and then with the help of accurate numerical methods [22]. It was found that, approximately, half of the GSs are stable, and the other half unstable (the solitons with positive and negative intrinsic frequencies, respectively); the position of the stability border very weakly depends on the soliton's velocity, c [22] (in the present notation, the velocity takes values $|c| < 1$). Recently, the analysis was extended to GSs in a model with saturable (rather than cubic) nonlinearity [23].

A general stationary-wave solution to Eqs. (1) is looked for as

$$U(x,t) = u(x)\exp(-i\omega t), \quad V(x,t) = v(x)\exp(-i\omega t), \quad (2)$$

with frequency ω. Equations produced by the substitution of these expressions in Eqs. (1) admit the well-known reduction $v(x) = -u^\star(x)$. Then, complex function $u(x)$ is sought for in the Madelung form

$$u(x) = R(x)\exp[i\Psi(x)/4] \quad (3)$$

(factor 1/4 in front of phase Ψ is introduced to simplify subsequent expressions). It is easy to check that the amplitude may be eliminated in favor of the phase

$$R(x) = \sqrt{(1/6)[\Psi' - 4\omega + 4\kappa \cos(\Psi/2)]} \quad (4)$$

($\Psi' \equiv d\Psi/dx$), and the phase obeys the stationary version of the double sine-Gordon equation

$$\Psi'' = 8\kappa\omega \sin(\Psi/2) - 4\kappa^2 \sin\Psi. \quad (5)$$

A. Periodic waves of the "sn" type

Equation (5) is integrable in terms of the Jacobi's elliptic functions. One family of such exact periodic solutions can be found in the form of

$$\Psi(x) = 4 \tan^{-1}\left[\frac{\sqrt{2}rk \ \text{sn}(rx)}{\sqrt{4\kappa\omega + 4\kappa^2 - r^2(1+k^2)}}\right], \quad (6)$$

where k, taking values $0 < k < 1$, is the modulus of the elliptic sine (sn), r is an arbitrary real constant, and the corresponding frequency is

$$\omega = \pm (4\kappa)^{-1}\sqrt{[4\kappa^2 - r^2(1+k^2)]^2 - 4r^4k^2}. \quad (7)$$

Thus, solution family (6) contains two independent parameters k and r, which determine ω as per Eq. (7). The condition that the expressions under the square roots in Eqs. (6) and (7) must be positive imposes the following restrictions on the parameters

$$4\kappa^2 > r^2(1+k)^2, \quad (8)$$

i.e., the sn-type solutions exist provided that the Bragg reflectivity is not too small. Although similar periodic solutions
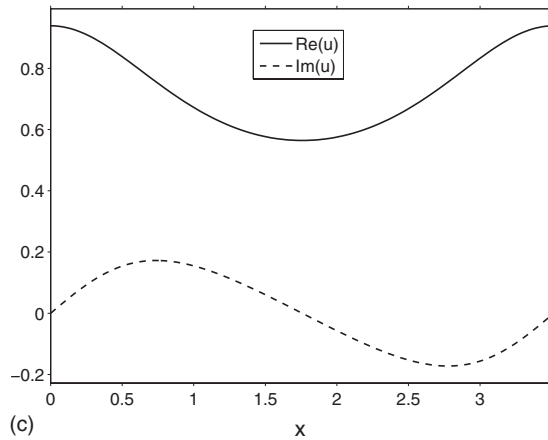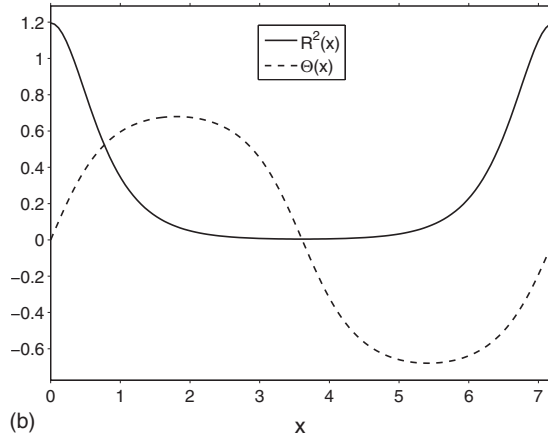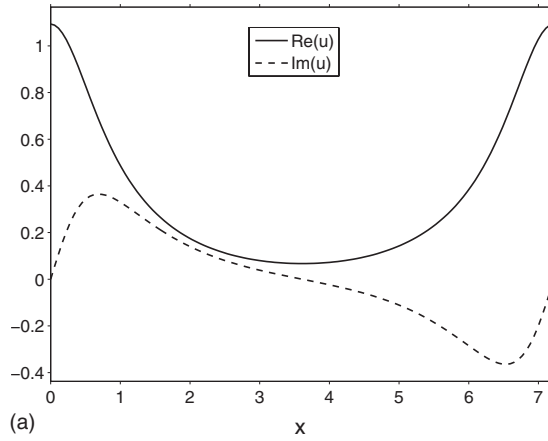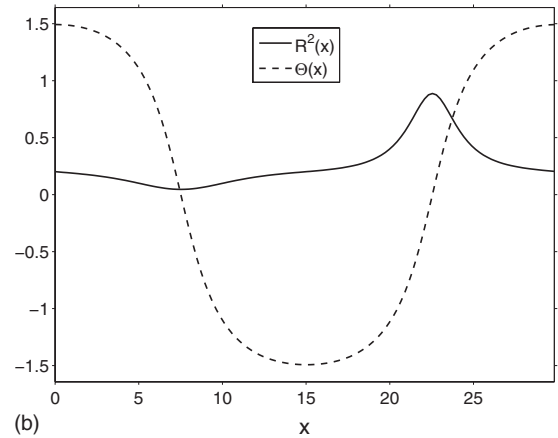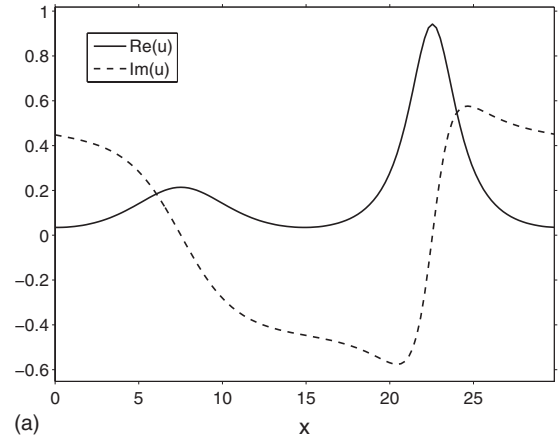
FIG. 2. An example of the periodic-wave solution of the cn type. Panels (a) and (b) have the same meaning as in Fig. 1. Parameters are $\omega = -0.5$, $k = 0.995$, $\kappa = 0.2$, and $r = 0.4919$.

tion for r^2, one can check that only one root complies with condition (8),

$$r^2 = \frac{4\kappa^2(1+k^2)}{(1-k^2)^2} - 4\kappa^2 \sqrt{\frac{(\omega/\kappa)^2 - 1}{(1-k^2)^2} + \frac{(1+k^2)^2}{(1-k^2)^4}}. \quad (9)$$

It immediately follows from Eq. (9) that condition $r^2 > 0$ implies that the frequency may only take values from interval $\omega^2 < \kappa^2$, i.e., as might be expected, the solutions may exist only inside the bandgap $-\kappa < \omega < \kappa$. Typical examples of the sn-type stationary periodic solutions, as given by Eq. (6), are displayed in Fig. 1, for large [(a),(b)] and small (c) values of elliptic modulus k, which represent the long- and short-period waves, respectively.

B. Periodic waves of the "cn" type

Another family of exact solution to Eq. (5) can be found in the form

$$\Psi = 4 \tan^{-1}\left[\frac{\sqrt{2}rk \ \mathrm{cn}(rx)}{\sqrt{r^2(1-2k^2) - 4\kappa^2 - 4\kappa\omega}}\right], \quad (10)$$

FIG. 1. Examples of periodic-wave solutions of the sn type. Cases $\omega = 0.1$, $k = 0.8$, $\kappa = 1$, and $r = 1.055$ (a), (b), and $\omega = 0.1$, $k = 0.1$, $\kappa = 1$, and $r = 1.792$ (c) represent long- and short-period waves, respectively. In (a) and (c), real and imaginary parts of stationary field $u(x)$ are shown within one period. In (b), amplitude $R(x)$ and phase $\Theta \equiv \Psi(x)/4$ are additionally shown for the long-wave solution.

have been reported earlier [3,8,24], the present formulas offer certain advantages, as described below.

For the subsequent analysis, it is convenient to use κ and ω as free parameters, therefore we invert Eq. (7) to express r^2 in terms of κ and ω. Solving the resulting quadratic equa-

$$\omega = -(4\kappa)^{-1}\sqrt{[r^2(1-2k^2) - 4\kappa^2]^2 + 4r^4k^2(1-k^2)}. \quad (11)$$

To ensure that the solution is real, only the negative sign in front of the square root in Eq. (11) must be taken, i.e., the cn-type solution, unlike its sn counterpart, given by Eqs. (6) and (7), exists only at negative frequencies. On the other hand, the presence of the radicals in Eqs. (10) and (11) does not impose any additional constraint on the existence range for this solution. Further, examination of expression (11) reveals that $|\omega|$ may exceed κ, i.e., the cn family is not restricted to the (lower half of) the gap. In particular, the cn-wave solution is located outside the gap, provided that

$$r^2 > 8\kappa^2(1-2k^2). \quad (12)$$

Precisely at the edge of the gap, i.e., for $r^2 = 8\kappa^2(1-2k^2)$ (which is tantamount to $\omega = -\kappa$), Eq. (10) yields

$$\Psi = 4 \tan^{-1}\left[\frac{\sqrt{2}k \ cn(rx)}{\sqrt{1-2k^2}}\right]. \quad (13)$$

It is interesting to note that all cn-type solutions with $k^2 > 1/2$ reside out of the gap, as seen from Eq. (12). A typical example of the cn-type stationary solution (with the frequency lying outside of the gap, although close to its edge) is shown in Fig. 2.

C. Long-wave limits of the sn and cn waves

The long-wave limit $k \to 1$ in the above solutions is of special interest, as it corresponds to states with the infinite period, among which GSs should appear. Indeed, Eqs. (6) and (9) with $k=1$ yield $r = \sqrt{\kappa^2 - \omega^2}$ and

$$\Psi = 4 \tan^{-1}\left[\frac{\sqrt{\kappa^2 - \omega^2} \ \tanh(\sqrt{\kappa^2 - \omega^2}x)}{\kappa + \omega}\right]. \quad (14)$$

The substitution of this expression in Eqs. (4) and (3) readily recovers the ordinary GS solution

$$u = 2\sqrt{\frac{2\kappa}{3}}\sin\theta\left[\frac{\cos(\theta/2)\cosh(\sqrt{\kappa^2 - \omega^2}x) + i \ \sin(\theta/2)\sinh(\sqrt{\kappa^2 - \omega^2}x)}{\cosh(2\sqrt{\kappa^2 - \omega^2}x) + \cos(\theta)}\right], \quad (15)$$

with θ related to ω and κ by $\cos\theta = \omega/\kappa$, $\sin\theta = \sqrt{\kappa^2 - \omega^2}/\kappa$. For k sufficiently close to 1, the periodic sn wave may be regarded as a chain of solitons, as suggested, for instance, by the plot of $R^2(x)$ in Fig. 1(b).

The long-wave limit for the cn-type solutions corresponds, as follows from Eq. (11), to $\omega = -(4\kappa)^{-1}(r^2 + 4\kappa^2)$ (in accordance with what was said above, this value lies outside of the spectral gap). To derive a relevant limit form of solution (10) corresponding to $k \to 1$, we first shift the coordinate, by defining $x \equiv x' \pm \mathbf{K}(k)$ ($\mathbf{K}$ is the complete elliptic integral of the first kind) while keeping $k \neq 1$, and then make use of relation $cn[z \mp \mathbf{K}(k)] = \pm\sqrt{1-k^2}sn(z)/dn(z)$. Then, the limit form of solution (10) reduces to phase kinks

$$\Psi = \pm 4 \tan^{-1}\left[\sqrt{1 + \frac{4\kappa^2}{r^2}}\sinh(rx')\right], \quad (16)$$

which connect values $\Psi = \pm 2\pi$ at $x' = \pm\infty$. As follows from Eq. (4), the amplitude profiles corresponding to kinks (16) with the upper and lower signs represent, respectively, antidark and dark solitons. In either case, the background field at $x' = \pm\infty$ is $R_\infty = r/\sqrt{6\kappa}$, and the local amplitude at the central point $x' = 0$ is $R_0 = (\sqrt{4\kappa^2 + r^2} \pm 2\kappa)/\sqrt{6\kappa}$. Obviously, this yields $R_0 > R_\infty$ for the antidark soliton and $R_0 < R_\infty$ for its dark counterpart. Solutions for the dark and antidark solitons were found before [25], but they are unstable, because the uniform background supporting both of them is subject to the modulational instability [17].

The periodic waves of the cn type, with k close to 1, may be understood as chains composed of periodically alternating dark and antidark solitons. This interpretation is suggested, in particular, by Fig. 2(b). Note that the dark and antidark solitons always lie outside of the bandgap, because, as shown above, all cn solutions with $k^2 > 1/2$ reside at $|\omega| > \kappa$.

A remark on the relation between the present results and earlier ones for periodic waves in FBG [3–6,8,24] is in order. Previous presentations employed Stokes parameters to obtain the solution in an implicit form, expressing the spatial coordinate as an elliptic integral of the local intensity. In terms of this approach, roots of a fourth-order polynomial, that determines the form of the elliptic integral, must first be determined (in fact, numerically, as analytical expressions for them are extremely cumbersome) to relate the solution to physical parameters, such as frequency ω and reflectivity κ. The present calculations directly express the solutions in terms of these parameters, and also give the phase of the electric field in a straightforward manner, which was inaccessible in earlier formulations. Furthermore, the present calculations readily reproduce the known bright, dark, and antidark solitons [Eqs. (14)–(16)], while the earlier formulations might have difficulties with this. In fact, in the long-wave limit (with the elliptic modulus of sn approaching 1), the abovementioned fourth-order polynomial, which determines the previously known periodic solutions, exhibits multiple roots, which gives rise to indefinite expressions or constant solutions.

III. NUMERICAL RESULTS: UNSTABLE AND ALMOST STABLE SOLUTIONS

As mentioned above, only half of the soliton family (15) is stable, namely, the part with $\omega > 0$ (i.e., $\theta < \pi/2$), while

the other half, with $\pi/2 < \theta < \pi$, is unstable [strictly speaking, the stability border is located at $\theta \approx 1.01(\pi/2)$, rather than exactly at $\theta = \pi/2$ [22]]. Here, we aim to examine the stability of the periodic solutions presented above, by computing the corresponding eigenvalues of small perturbations, and using direct simulations.

A. Linear stability analysis

Perturbed solutions of underlying Eqs. (1) are looked for as

$$U = [u_0(x) + u_1(x)e^{-i\lambda t}]e^{-i\omega t}, \quad V = [v_0(x) + v_1(x)e^{-i\lambda t}]e^{-i\omega t},$$
(17)

where $u_0(x)$ and $v_0(x)$ are the stationary solutions, as defined above, while $u_1(x)$ and $v_1(x)$ are eigenmodes of small perturbations with respective instability growth rate $-i\lambda$. The substitution of the perturbed solutions in Eqs. (1) and the linearization lead to the system of ordinary differential equations

$$\left(\omega + i\frac{d}{dx}\right)u_1 + (|u_0|^2 + |v_0|^2)u_1 + \frac{1}{2}u_0^2 v_1^*$$

$$+ u_0(v_0^* v_1 + v_0 v_1^*) + \kappa v_1 = -\lambda u_1,$$

$$\left(\omega - i\frac{d}{dx}\right)v_1 + (|u_0|^2 + |v_0|^2)v_1 + \frac{1}{2}v_0^2 v_1^* + v_0(u_0^* u_1 + u_0 u_1^*)$$

$$+ \kappa u_1 = -\lambda v_1.$$
(18)

To obtain a closed system, we add to Eqs. (18) their complex-conjugate version, formally treating u_1 and u_1^*, and v_1 and v_1^* as independent functions. Eigenvalues λ, along with the associated eigenfunctions $u_1(x)$ and $v_1(x)$, were found from numerical solution of this linear system.

Examples of spectra of the numerically computed instability growth rate, which is defined as the maximum value of $\mathrm{Im}(\lambda)$ for a given solution of the sn type (for solutions of the cn type, the instability is much stronger, because of the abovementioned modulational instability of the segments with the nearly constant amplitude, separating the dark and antidark solitons, of which the cn wave is built, see Fig. 2), are presented in Fig. 3. Results shown in this figure are incomplete, as they were obtained from solutions of Eqs. (18) which have the same periodicity as the unperturbed sn wave. Nevertheless, these partial results show a correct trend: as the separation between individual solitons that build the chain increases, i.e., k (the elliptic modulus) approaches 1, and the period of solution (6), $4\mathbf{K}(k)/r$, grows as $\ln[1/(1-k^2)]$, the entire pattern becomes more stable. This trend can be easily understood, as the individual solitons are stable, if taken in isolation, while the interaction between them, that may lead to instability, is exponentially small if the separation between them is large. Practically speaking, it is possible to identify a particular value of $1-k$, such as $k \approx 0.9$ in Fig. 3(b), past which the instability virtually disappears.

It may also be relevant to mention that these stability results will be complete if applied to an FBG loop (rather than a linear piece of the fiber), which imposes periodic boundary conditions. Loop-shaped FBGs were considered, in
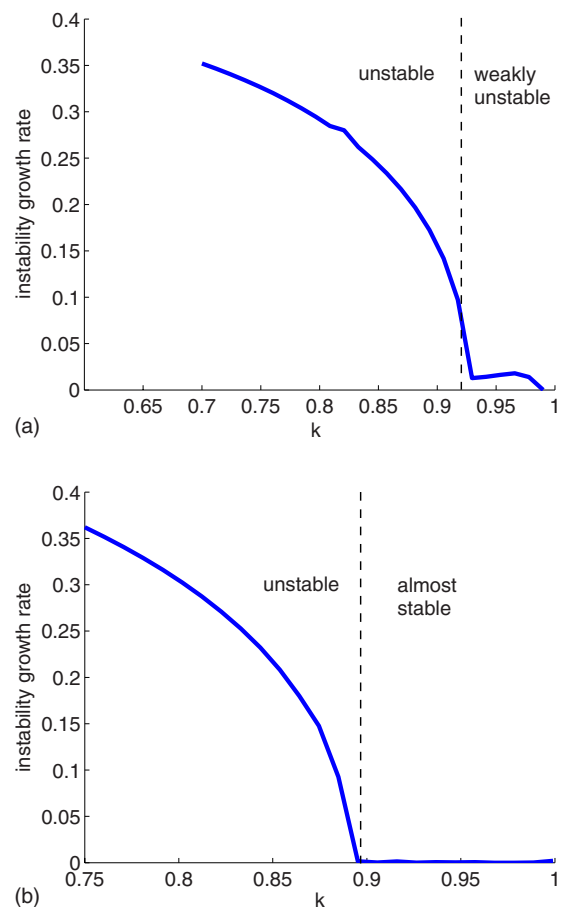

FIG. 3. (Color online) The instability growth rate for two families of the sn-type periodic solutions, at fixed values of $\omega = 0.3$ (a) and $\omega = 0.1$ (b), as a function of elliptic modulus k. The results were obtained from numerical solution of linearized Eqs. (18), confined to perturbations with the same period as the unperturbed solution.

particular, in Ref. [15], where multiple collisions between moving solitons in the ring geometry were discussed. The FBG loop may serve as a basis for the design of fiber lasers, which could deserve special consideration. In physical units, examples of the periodic solutions displayed in Figs. 1 and 2 correspond to the period on the order of few centimeters, which may be a realistic size for the FBG loops (thus making the potential ring-shaped FBG lasers quite compact).

B. Direct simulations

The above results demonstrate that the sn-type waves with a sufficiently large period may be practically stable, which suggests to test the stability of the waves in direct simulations of Eqs. (1). The simulations were performed by means of the split-step Fourier method. As the sn-type waves are expected to be essentially less unstable than their cn-type counterparts, we will chiefly focus on solutions of the former type; the cn waves will be briefly considered at the end of this subsection.

Direct simulations corroborate the prediction of the linear-stability analysis: the instability of the sn waves, with $\omega > 0$, quickly weakens as k approaches 1, making the period
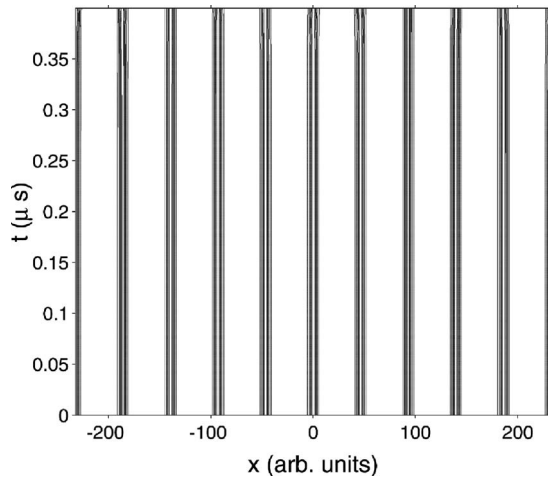
FIG. 4. Onset of a very weak instability of the periodic sn-type wave. Here (as well as in Figs. 6 and 7 below), only the u component is shown (by means of contour plots), as the respective picture in the v component is very similar. Parameters of the unperturbed solutions are $k=0.99$, $\omega=0.8$, $\kappa=0.85$, and $r=0.2887$.

of the wave larger. A typical run of the simulations for a long-period wave is displayed in Fig. 4, where small initial perturbations develop into barely visible irregularities in the periodic pattern only at $t \gtrsim 4 \times 10^4$, which corresponds to $\sim 0.5 \ \mu$s, in physical units (a long time, in terms of optics).

Collecting results produced by many runs of the simulations, we have identified the time of the onset of the instability $t_{\text{instability}}$ as a function of the natural intrinsic parameter of the solution family $1-k$. The results are plotted at fixed values of other parameters in Fig. 5. The plots corroborate the expectation that the instability is strongly attenuated with the increase of the period of the sn wave. The waves also become more stable, for fixed k, as one approaches the edge of the bandgap, increasing ω toward $\omega=\kappa$, see Fig. 5(a), or decreasing κ toward $\kappa=\omega$, see Fig. 5(b). The latter trend can be easily understood: Eq. (9) shows that r vanishes in the limit of $\omega/\kappa \to 1$, hence solution (6) becomes nearly linear (its amplitude also vanishes $\sim r$), while the instability of the sn wave is a nonlinear effect.

As mentioned above, GSs in the standard FBG model are unstable in the lower half of the bandgap, at $\omega < 0$, and the periodic sn solutions share this property, as illustrated by an example displayed in Fig. 6. Comparing it with Fig. 4, we conclude that the sn waves with negative frequencies develop the instability, roughly speaking, 100 times faster than their robust counterparts with $\omega > 0$. This difference can be readily explained, as in the case of $\omega < 0$ the individual solitons, which build the sn pattern, are intrinsically unstable by themselves.

Direct numerical simulations of the cn-wave solutions were performed too (for $\omega < 0$, since they do not exist otherwise, as shown above). A typical example, presented in Fig. 7, demonstrates that the cn waves are still more unstable than their sn counterparts with $\omega < 0$.

IV. CONCLUSION

We have found two families of exact periodic solutions for the standard FBG model, of the sn and cn types. The
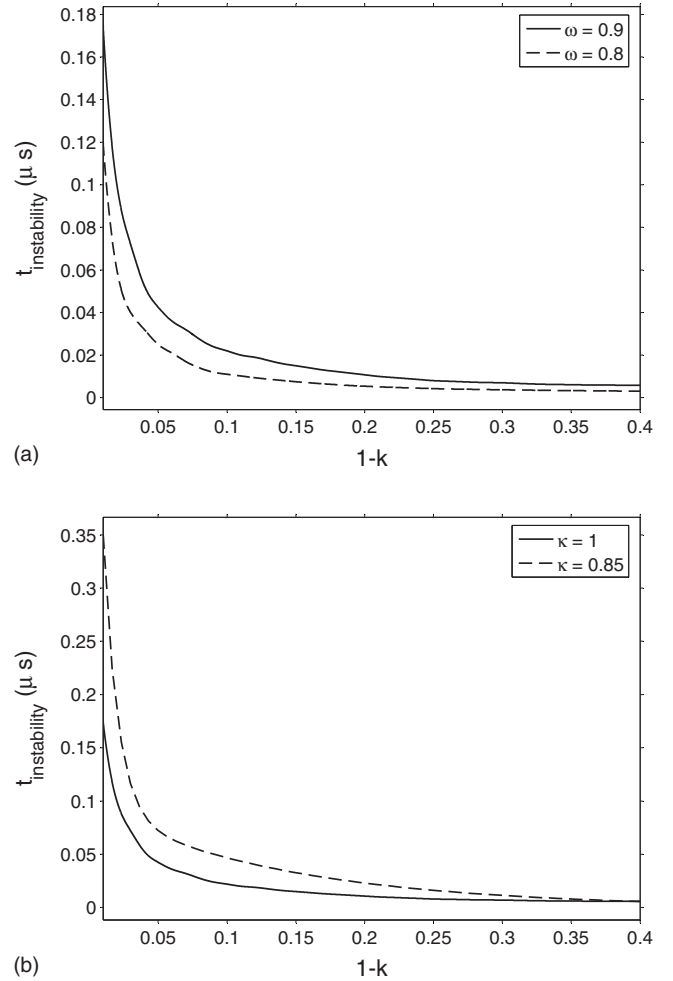

FIG. 5. The instability-onset time for sn-type waves versus $1-k$, with the fixed Bragg reflectivity $\kappa=1$ at different frequencies ω (a) and with fixed $\omega=0.9$ at different κ (b). Time $t=10\,000$ corresponds, in physical units, to $\sim 0.1 \ \mu$s.

presentation of the solutions is different from and more compact than given in earlier works. In the long-wave limit, the sn solutions (which exist only inside the spectral gap) go over into the ordinary GS (gap soliton), while the cn solutions take the form of previously known (unstable) out-of-the-gap antidark and dark solitons. Stability of both classes of the solutions was tested in direct simulations, and, for the sn-type solutions, the instability growth rate was also found from linearized equations for small perturbations. Strictly speaking, all periodic solutions are unstable. However, for the solutions of the sn type, with positive frequencies ($\omega > 0$) and a large spatial period, the instability is very weak, and the analysis of the eigenvalues, along with results of direct simulations, make it possible to identify a subclass of the sn waves which are very robust (practically stable). These robust periodic waves may be observed in the experiment—either in the ordinary form of the transmission function or, plausibly, as dynamical states in an FBG loop, that may be a basis for the design of a ring-shaped fiber laser. On the other hand, the sn solutions with $\omega < 0$ are strongly unstable. As concerns periodic solutions of the cn type, they
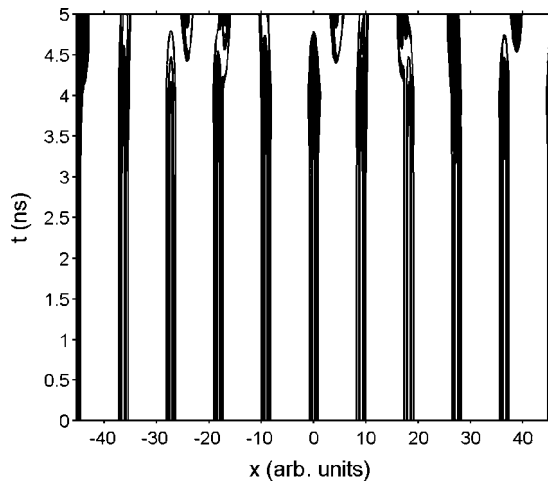
FIG. 6. The instability of the sn wave at a negative frequency: $\omega=-0.3$, $k=0.9$, $\kappa=1$, and $r=1.004$. Note that in this figure and in Fig. 7, the actual time unit is nanosecond, unlike microsecond in Fig. 4.
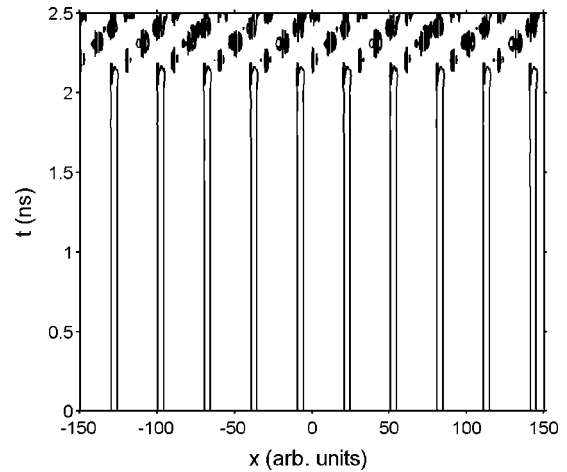

FIG. 7. Strong instability of a cn wave with $k=0.995$, $\kappa=0.2$, $r=0.492$, and $\omega=-0.5$. Note that this ω lies outside of the bandgap ($|\omega|>|\kappa|$).

exist only at $\omega<0$ and were found to be strongly unstable too.

It is relevant to mention that the explicit solutions of the double sine-Gordon equation reported in this paper may also be applicable in other fields of physics, where this equation is relevant. These potential applications include spin waves in antiferromagnetic materials [26], Heisenberg spin chains [27], and some models of hadron matter [28].

[1] R. Kashyap, *Fiber Bragg Gratings* (Academic Press, San Diego, 1999).

[2] B. A. Malomed, *Soliton Management in Periodic Systems* (Springer, New York, 2006).

[3] H. G. Winful, J. H. Marburger, and E. Garmire, Appl. Phys. Lett. **35**, 379 (1979).

[4] H. G. Winful, Phys. Rev. Lett. **49**, 1179 (1982).

[5] H. G. Winful and J. H. Marburger, Appl. Phys. Lett. **36**, 613 (1980).

[6] Yu. A. Logvin and V. M. Volkov, J. Opt. Soc. Am. B **16**, 774 (1999).

[7] H. G. Winful, Appl. Phys. Lett. **46**, 527 (1985).

[8] Yu. I. Voloshchenko, Yu. N. Ryzhov, and V. E. Sotin, Zh. Tekh. Fiz. **51**, 902 (1981) [Sov. Phys. Tech. Phys. **26**, 541 (1981)].

[9] W. Chen and D. L. Mills, Phys. Rev. Lett. **58**, 160 (1987).

[10] D. L. Mills and S. E. Trullinger, Phys. Rev. B **36**, 947 (1987).

[11] D. N. Christodoulides and R. I. Joseph, Phys. Rev. Lett. **62**, 1746 (1989).

[12] A. B. Aceves and S. Wabnitz, Phys. Lett. A **141**, 37 (1989).

[13] B. J. Eggleton, R. E. Slusher, C. M. de Sterke, P. A. Krug, and J. E. Sipe, Phys. Rev. Lett. **76**, 1627 (1996); B. J. Eggleton, C. M. de Sterke, and R. E. Slusher, J. Opt. Soc. Am. B **16**, 587 (1999).

[14] J. T. Mok, C. M. de Sterke, I. C. M. Littler, and B. J. Eggleton, Nat. Phys. **2**, 775 (2006).

[15] W. C. K. Mak, B. A. Malomed, and P. L. Chu, Phys. Rev. E **68**, 026609 (2003).

[16] H. G. Winful, R. Zamir, and S. Feldman, Appl. Phys. Lett. **58**, 1001 (1991).

[17] C. M. de Sterke, J. Opt. Soc. Am. B **15**, 2660 (1998).

[18] H. G. Winful and G. D. Cooperman, Appl. Phys. Lett. **40**, 298 (1982).

[19] C. M. de Sterke and J. E. Sipe, Prog. Opt. **33**, 203 (1994).

[20] W. C. K. Mak, B. A. Malomed, and P. L. Chu, J. Mod. Opt. **51**, 2141 (2004).

[21] B. A. Malomed and R. S. Tasgal, Phys. Rev. E **49**, 5787 (1994).

[22] I. V. Barashenkov, D. E. Pelinovsky, and E. V. Zemlyanaya, Phys. Rev. Lett. **80**, 5117 (1998); A. De Rossi, C. Conti, and S. Trillo, *ibid.* **81**, 85 (1998).

[23] I. M. Merhasin, B. A. Malomed, K. Senthilnathan, K. Nakkeeran, K. A. Wai, and K. W. Chow, J. Opt. Soc. Am. B **24**, 1458 (2007).

[24] K. Senthilnathan, P. Malathi, and K. Porsezian, J. Opt. Soc. Am. B **20**, 366 (2003).

[25] J. Feng and F. K. Kneubühl, IEEE J. Quantum Electron. **29**, 590 (1993).

[26] J. A. Holyst and H. Benner, Phys. Rev. B **52**, 6424 (1995).

[27] A. Saxena and R. Dandoloff, Phys. Rev. B **58**, R563 (1998); R. Dandoloff and A. Saxena, Eur. Phys. J. B **29**, 265 (2002).

[28] M. Fabrizio, A. O. Gogolin, and A. A. Nersesyan, Nucl. Phys. B **580**, 647 (2000); H. Blas and H. L. Carrion, J. High Energy Phys. **2007**, 027 (2007).